



**HAL**  
open science

# The Prediction of Necking and Failure in 3 D. Sheet Forming Analysis Using Damage Variable

M. Brunet, F. Sabourin, S. Mguil-Touchal

► **To cite this version:**

M. Brunet, F. Sabourin, S. Mguil-Touchal. The Prediction of Necking and Failure in 3 D. Sheet Forming Analysis Using Damage Variable. Journal de Physique IV Proceedings, 1996, 06 (C6), pp.C6-473-C6-482. 10.1051/jp4:1996647 . jpa-00254480

**HAL Id: jpa-00254480**

**<https://hal.science/jpa-00254480>**

Submitted on 4 Feb 2008

**HAL** is a multi-disciplinary open access archive for the deposit and dissemination of scientific research documents, whether they are published or not. The documents may come from teaching and research institutions in France or abroad, or from public or private research centers.

L'archive ouverte pluridisciplinaire **HAL**, est destinée au dépôt et à la diffusion de documents scientifiques de niveau recherche, publiés ou non, émanant des établissements d'enseignement et de recherche français ou étrangers, des laboratoires publics ou privés.

## The Prediction of Necking and Failure in 3 D. Sheet Forming Analysis Using Damage Variable

M. Brunet, F. Sabourin and S. Mguil-Touchal

*Laboratoire de Mécanique des Solides, INSA, Bâtiment 304, 69621 Villeurbanne, France*

**Abstract:** The modeling of necking occurrence in sheet metal forming is a real challenge for the engineer concerned with processing of new geometries and materials. As fracture in metal forming is mainly due to the development of ductile damage and to represent the failure of anisotropic sheet-metals, an extension of the Gurson-Tvergaard model is presented and implemented in the context of plane-stress for shell elements. A one dimensional problem is solved and compared with the exact solution of the literature. The paper closes with a numerical and experimental study of the necking of a square cup deep-drawing using the modified Gurson's model to described the constitutive behavior of the material. Finally, a numerical necking criterion is proposed.

### 1. INTRODUCTION

There are several ways to achieve analysis of necking occurrence in sheet-metal forming. One way consists in carry out a conventional F.E. simulation and by postprocessing the F.E. results, in using a theoretical or experimental necking criterion, to detect the zones where risks of necking can occur. It is the approach we have employed in [1] and [2] introducing the concept of Forming Limit Stress Surfaces for anisotropic sheets. It has been found that the Forming Limit Stress Diagrams are much more intrinsic than the conventional F. L. Strain Diagrams strongly influenced by the strain path which may vary significantly from the direct strain path in the case of complex sheet-metal forming processes. If experimental F.L.D. are not available, the strains of elements calculated in every steps by F.E. analysis are compared with the necking limits obtained by formulas based on plastic-instability theories such that the Stor en-Rice criterion [3]. However, many Limiting Dome Height (L.D.H.) tests [4] on steel-sheets have shown that theoretical formulas give smaller heights than the measured values, except for aluminum alloys.

On the other hand, a large number of macroscopic fracture criteria for failure which occurs after necking have been evaluated by Doege and co-workers [5],[6], consisting of products, integrals and sums of macroscopic stresses and strains. To determine the values of these criteria at the onset of failure, both experiments and F.E. simulations are needed. When applying these criteria, it was found that the main factor affecting the accuracy is the mode in which failure takes place, mainly under deep-drawing or under stretching conditions. The equivalent Mises stress was judged best for the prediction of both deep-drawing and stretch-drawing cracks but the locus of maximum equivalent stress does not necessarily coincides with the locus of failure in the sheet [6]. Moreover, the thickness distribution may also indicate the wrong locus of failure since this parameter is operation dependant and there is no material dependant critical sheet thickness reduction.

Since deformation after necking up to fracture consists of sheet thinning within the neck together with complementary tensile stretching perpendicular to the neck and no straining along the neck, in many forming operations, the onset of necking is considered to be limiting. Also there is a need in the simulation process to achieve better localization of the onset of necking. This can be expected by the coupled approach where the damage process is incorporated into the constitutive relations. Many investigations have shown that ductile fracture involves four successive damage processes which are the nucleation of voids from inclusions, void growth, void coalescence and cracking propagation. One constitutive equation to account for these processes is the Gurson-Tvergaard model [7],[8], which was derived in an attempt to model a porous isotropic plastic material containing randomly disposed voids. As suggested by Doege and co-workers [9], we have extended the Gurson-Tvergaard model to anisotropic matrix behavior and implemented with our

simplified triangular shell element suitable for simulating sheet-metal forming processes [10]. After localization by the iso-value curves of the porosity which acts as an macroscopic internal damage variable, the onset of necking may be found numerically by geometrical considerations due to the fact that the stress state becomes triaxial in the neck. Comparisons between experiments and coupled numerical analysis of a square cup deep-drawing of an anisotropic steel-sheet are presented.

## 2. DAMAGE MODEL

The proposed damage model is based on an extension of the Gurson-Tvergaard model [7],[8] in which microvoid volume fraction evolution in the constitutive matrix is described. The proposed yield condition takes the form :

$$\Phi = q^2/\sigma_y^2 + 2q_1 f \cosh(-3q_2 p/2\sigma_y) - (1 + q_3 f^2) = 0 \quad (1)$$

if  $\sigma_m = -p > 0$  where  $p$  is the hydrostatic pressure and :

$$\Phi = q^2/\sigma_y^2 + 2q_1 f - (1 + q_3 f^2) = 0 \text{ if } \sigma_m \leq 0 \quad (2)$$

$f$  is the state variable available for microvoided material, called microvoid volume fraction or porosity and defined by :

$$f = (V_A - V_M) / V_A \quad (3)$$

with  $V_A$  elementary apparent volume of material and  $V_M$  the corresponding matrix one. In relations (1) and (2)  $q$  is the effective stress of the macroscopic Cauchy stress tensor  $\sigma$  which, instead of the original Mises stress is replaced by the orthotropic Hill effective stress :

$$q^2 = \sigma^T \mathbf{M} \sigma \quad (4)$$

where for plane-stress condition and in the orthotropic axes 1 and 2 :

$$\sigma^T = \begin{bmatrix} \sigma_{11} & \sigma_{22} & \sigma_{12} \end{bmatrix} \quad \text{and} \quad \mathbf{M} = \begin{bmatrix} G+H & -H & 0 \\ -H & F+H & 0 \\ 0 & 0 & 2N \end{bmatrix} \quad (5)$$

The anisotropic plastic behavior of the metal is described by the anisotropy parameters  $G, H, F$  and  $N$  which are defined in terms of the Lankford parameters  $r_0, r_{90}$ , and  $r_{45}$  as :

$$H = r_0/(1+r_0) \quad G = 1-H \quad F = r_0/[r_{90}(1+r_0)] \quad N = (r_{90}+r_0)(2r_{45}+1)/[2r_{90}(1+r_0)] \quad (6)$$

The Lankford parameters are determined by three experiments in the various directions as pointed out by their different indices. This model is often preferred for industrial applications with steel sheets. If  $H=G=F=1/2$  and  $N=3/2$  Eq.(4) abridges to standard Mises isotropy. Due to the Hill function and the associated flow rule not being isotropic, the direct Eulerian constitutive law based on this criterion is not objective. In order to assure the objectivity, the rotating frame formalism is applied. The axes of orthotropy of the Hill criterion can be updated by a rotation which can be chosen as the material spin rate  $\omega$  (co-rotational stress rate) or from the polar decomposition  $F=RU$  (Green-Nagdi stress rate). Since the elastic strain are assumed to be small and from practical sheet forming applications, the differences between these different rotations are very small.

Tvergaard [8] introduced the constant  $q_1, q_2$  and  $q_3=q_1^2$  as coefficients of the void volume fraction and pressure terms in order to make the predictions of the Gurson model agree with numerical studies of ordered voided materials in plane strain tensile fields, typically :  $q_1=1.5$   $q_2=1$  and  $q_3=2.25$  instead of  $q_1=q_2=q_3=1$  in the original Gurson model. The flow rule is derived from the yield potential Eq.(1) and (2), the presence of the hydrostatic pressure in the yield function results in non-deviatoric plastic strains :

$$d\epsilon^P = d\lambda \frac{\partial \Phi}{\partial \sigma} = d\lambda \left[ \frac{\partial \Phi}{\partial p} \frac{\partial p}{\partial \sigma} + \frac{\partial \Phi}{\partial q} \frac{\partial q}{\partial \sigma} \right] \quad (7)$$

The hardening of the fully dense matrix material is described through  $\sigma_y = h(\bar{\epsilon}^P)$ . The evolution of  $\bar{\epsilon}^P$  is assumed to be governed by the equivalent plastic work relation :

$$(1-f) \sigma_y d\bar{\epsilon}^P = \sigma^T d\epsilon^P \quad (8)$$

The damage model takes into account the three main phases of damage evolution. The microvoid volume fraction is given by :

$$df = df_N + df_c + df_c \quad (9)$$

Considering a random distribution of second phase particles, microvoid volume fraction increment due to nucleation is expressed by [13]:

$$df_N = \frac{f_N}{S_N \sqrt{2\pi}} \exp \left\{ -\frac{(\epsilon^p - \epsilon_N)^2}{2S_N^2} \right\} d\epsilon^p \quad (10)$$

The normal distribution of the nucleation strain has a mean value  $\epsilon_N$ , standard deviation  $S_N$  and nucleates voids with volume fraction  $f_N$ . For steel-sheet metals the possible values are  $f_N=0.04$ ,  $0.01 \leq S_N \leq 0.1$  and  $0.3 \leq \epsilon_N \leq 0.7$  [13]. Growth of existing voids is based on the apparent volume change and the law of conservation of mass and is expressed as :

$$df_G = (1-f) (d\epsilon_{11}^p + d\epsilon_{22}^p + d\epsilon_{33}^p) \quad (11)$$

Finally, it is assumed that the volume fraction increment due to coalescence depends on effective plastic strain increment such that :

$$df_C = A d\epsilon^p \text{ if } f \geq f_{CR} \text{ and } df_C = 0 \text{ if } f < f_{CR} \quad (12)$$

where  $f_{CR}$  is the critical fraction at incipient coalescence and A a material parameter which can be written as :

$$A = (f_U - f_{CR}) / \Delta\epsilon_E \quad (13)$$

where  $f_U$  is the ultimate microvoid volume fraction at ductile rupture and  $\Delta\epsilon_E$  is the additional effective strain increment leading to ductile rupture. It is worth noticing that if the damage evolution takes place in small areas as in the case of sheet metal forming, large values of porosity up to 25% can be only found on a micro level.

### 3. COMPUTATIONAL ASPECTS

#### 3.1 Explicit solution procedure

The three node simplified shell element [10] with only translational degree of freedom but with bending capability is adopted for the spatial discretization of the sheet. A large numbers of analysis have shown that sheet forming processes can be analyzed successfully by both the implicit static method and explicit dynamic procedure if the latter is run at a relatively low speed ( $\leq 10$  m/s). With the use of lumped mass matrix, the advantages of the explicit dynamic algorithm is that the stiffness matrix does not need to be formed and the contact conditions are modelled accurately in a simple manner because of the requirements of small time steps. Moreover the material behavior can be complex which is the case with internal damage variable leading to softening of the material.

#### 3.2 Integration of constitutive equations

It is known that one of the best algorithm for integrating constitutive equations is the Backward Euler or implicit scheme [11]. However, in case of plane-stress condition, the out of plane component of strain is not defined kinematically and must be added as an extra unknown in the local Newton iteration scheme. This fact and the presence of "cosh" terms in the yield function and flow rule may lead to numerical difficulties when the damage variable increases rapidly. The authors have chosen a substepping scheme on the modified Euler algorithm which incorporates error control where the details can be found in [12]. This approach is suitable with explicit dynamic analysis since it takes advantage of the small time step required by the overall stability limit.

Then on each substep, the following set of incremental forms of equations are used to compute the stress increments :

$$d\sigma = d\sigma^e - D d\epsilon^p \quad (14)$$

where  $d\sigma^e$  is the elastic stress increment vector and  $D$  the elastic (3x3) matrix satisfying the plane stress assumption. From the flow rule Eq.(7), the plastic multiplier  $d\lambda$  is eliminated with the following two equations :

$$\Delta\epsilon^p = -d\lambda \partial\Phi/\partial p \quad \text{and} \quad \Delta\epsilon^q = d\lambda \partial\Phi/\partial q \quad \text{with} \quad \Delta\epsilon^p \partial\Phi/\partial q + \Delta\epsilon^q \partial\Phi/\partial p = 0 \quad (15)$$

Eq.(1) and Eq.(2) are used to yield :

$$\Delta\epsilon^p = 0 \text{ if } \sigma_m \leq 0 \text{ and } \Delta\epsilon^p = \alpha \Delta\epsilon^q \text{ if } \sigma_m > 0 \quad \text{with} \quad \alpha = [3q_1 q_2 f \sinh(-3q_2 p / 2\sigma_y)] / 2q \quad (16)$$

Noticing the gradient vector  $\mathbf{a}$  so that :

$$\mathbf{a} = \partial q / \partial \sigma = \mathbf{q}^{-1} \mathbf{M} \sigma \quad \text{and} \quad \dot{d}\mathbf{q} = \mathbf{a}^T d\sigma = \mathbf{a}^T d\sigma^e - \beta \Delta \varepsilon^q \tag{17}$$

where it is found that for plane-stress :

$$\beta = \alpha E (a_{11} + a_{22}) / [3(1-\nu)] + \mathbf{a}^T \mathbf{D} \mathbf{a} \tag{18}$$

The equivalent plastic work Eq.(8) gives the effective strain increment :

$$d\bar{\varepsilon}^p = \Delta \varepsilon^q (q - \alpha p) / [(1-f)\sigma_Y] \tag{19}$$

Use of  $h' = d\sigma_Y / d\bar{\varepsilon}^p$  the hardening modulus of the matrix in Eq.(18) and in Eq.(19) leads to :

$$\Delta \varepsilon^q = \mathbf{a}^T d\sigma^e (1-f)\sigma_Y / [(h' + \gamma)(q - \alpha p)] \quad \text{where} \quad \gamma = \beta(1-f)\sigma_Y / (q - \alpha p) \tag{20}$$

The plastic out-of-plane strain increment can be now written as :

$$d\varepsilon_{33}^p = \alpha \Delta \varepsilon^q - (d\varepsilon_{11}^p + d\varepsilon_{22}^p) \tag{21}$$

Notice that if the porosity  $f=0$  then  $\alpha=0$  and the plastic incompressibility is obtained.

For the first order Euler algorithm, the stress at the end of a substep is given by :

$$\sigma_{K+1} = \sigma_K + d\sigma_1 \tag{22}$$

and it is the same for each internal state variable : the effective strain and porosity  $f$  where all quantities have been evaluated at the stress state  $\sigma_K$ . A more accurate estimate of  $\sigma_{K+1}$  and state variables may be obtained from the modified Euler scheme which gives :

$$\sigma'_{K+1} = \sigma_K + (d\sigma_1 + d\sigma_2) / 2 \tag{23}$$

where  $d\sigma_2$  and all quantities are evaluated at the stress state  $\sigma_{K+1}$ . The global error in the solution may be controlled by ensuring that the relative error for each substep is less than some specified tolerance :

$$\|(d\sigma_2 - d\sigma_1) / 2\| / \|\sigma_{K+1}\| < \text{TOL} \tag{24}$$

The size of each substep is continually updated during the integration procedure to satisfy Eq.(24) where TOL is a small positive number in the range 1.E-02 to 1.E-05 .

#### 4. NUMERICAL EXAMPLES

##### 4.1 Uniaxial tension

The first test is a uniaxial tensile test with two triangular shell elements making a unit square 4-node plane stress element. The test is velocity controlled with a tolerance factor  $\text{TOL}=1.E-05$  .

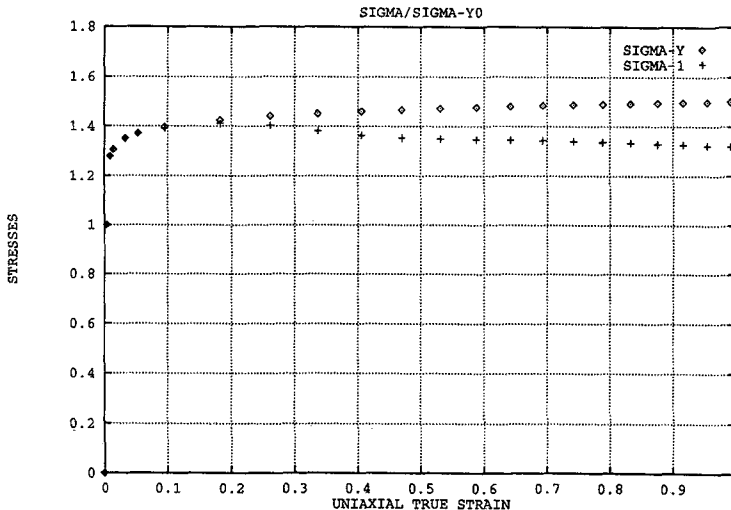


Figure 1 : Uniaxial stress-strain curves

The uniaxial stress-strain curve of the matrix is :  $\sigma_y = B(c + \bar{\epsilon}^p)^n$  with:  $B=1.5$  ,  $c=1.32775E-06$  and  $n=2.99633E-02$  .The elastic properties of the matrix material are specified by the ratio  $\sigma_{y0}=1/E=1/300$  and  $\nu=0.3$  . The plastic strain controlled nucleation is described by the void volume fraction  $f_N=0.04$  of void nucleating particles, the mean strain for nucleation  $\epsilon_N=0.3$  and the standard deviation  $S_N=0.1$  . The initial porosity is 0.001 . In Fig.(1) the  $\sigma_y$  and  $\sigma_{11}$  true stresses are plotted for each time interval  $\Delta t=1.E-02s$  as a function of the logarithmic strain  $\epsilon=\ln(1+u/l_0)$  where  $u=v\Delta t$  the prescribed displacement and  $l_0=1$  is the element length in the undeformed state. The void volume fraction  $f$  is plotted as a function of  $\epsilon$  in Fig.(2). The results of the finite element analysis agree very well with the finding of Aravas [11].

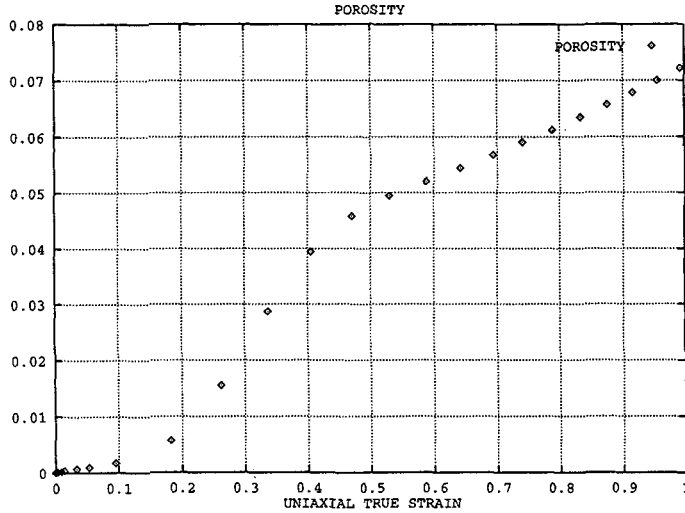


Figure 2 : Porosity versus uniaxial strain

### 4.2 Square-cup deep-drawing

The damage constitutive law is applied on a simulation of the deep-drawing of a square cup with dimensions according to the NUMISHEET'93 Benchmark where the geometry is given in Fig.(3) .

The material is a mild-steel sheet of thickness 0.67 mm with the following

properties  $\sigma_y = 533.38(1.8193E-03 + \bar{\epsilon}^p)^{0.1908}$   
 Young's modulus  $E = 198000$  MPa and Poisson's coefficient  $\nu=0.3$  with the anisotropic Hill's coefficients:  $H=0.654$   $G=0.346$   $F=0.317$   
 $N=1.220$  .Because the authors do not have the tools to perform the NUMISHEET'93 experiment,

it was Hoogovens Corporate Laboratory who have performed the experiment on their equipment. A square grid of 2.5 mm was applied to be able to measure the strain distribution of a product by mean of a video camera system.

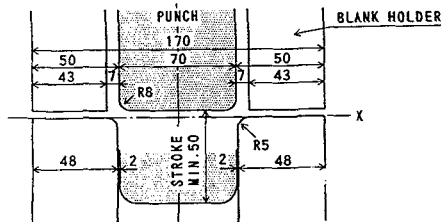


Figure 3 : Square-cup deep-drawing geometry

Hoogovens performed the following experiments:

- 1: Deep-drawing of a square-cup with a height of 26 mm and an applied blank holder force (B.H.F.) of 19.6 KN which correspond to a maximum punch force of 52.9 KN. The major and minor strain distribution are presented as they are measured on products in Fig.(4a).

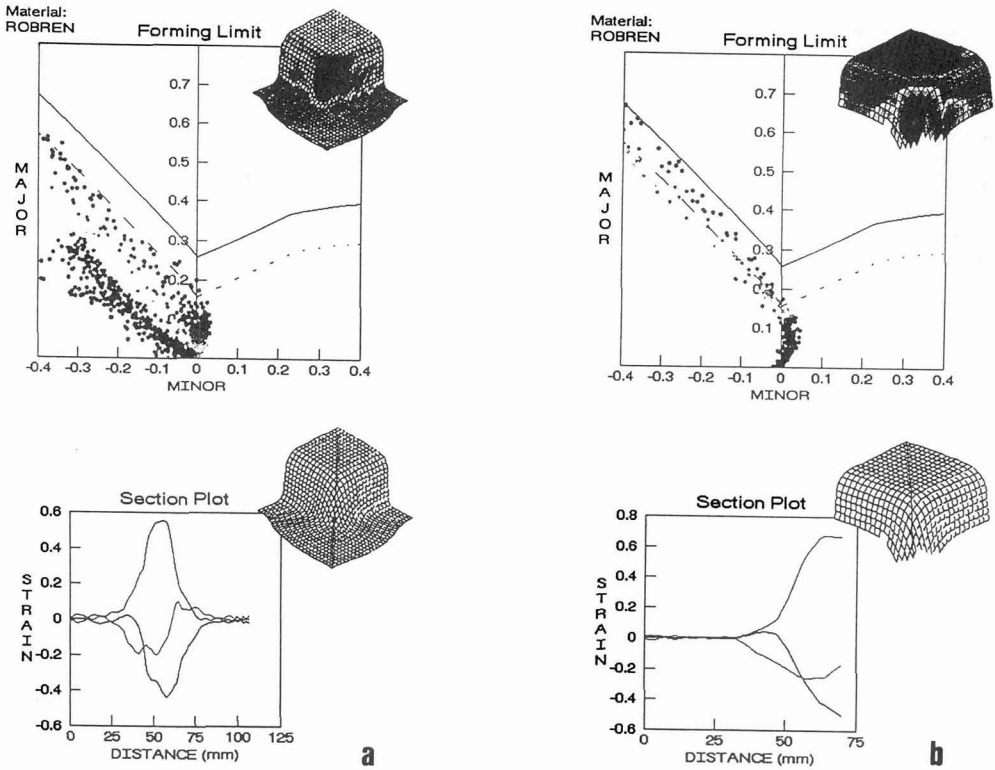


Figure 4 : Measured strain distribution (a) B.H.F. = 19.6 KN (b) B.H.F. = 70.0 KN

2: The blank holder force had to be raised to 70 KN before the first necking appeared to produce a cup with a height of 26 mm which corresponds to a maximum punch force of 59.7 KN. The major and minor strain distributions are presented as they are measured on product in Fig.(4b).

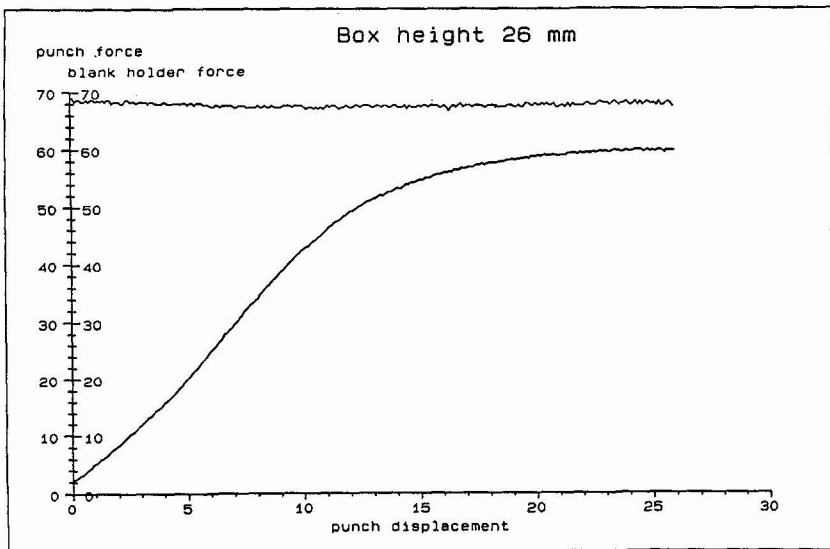


Figure 5(a): Experimental Punch force versus displacement

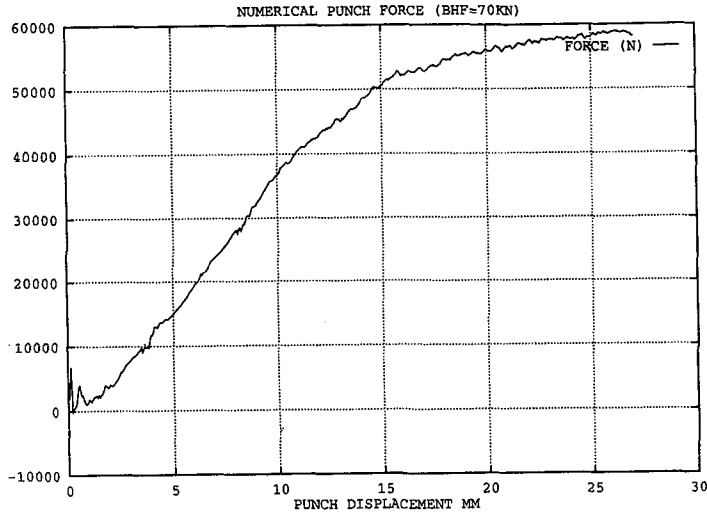


Figure 5(b): Numerical Punch force versus displacement

One quarter of the 150x150 mm square sheet was modelled by 1250 3-node simplified shell elements, with the tooling described by patches of surfaces (N.U.R.B.S.) generated with a C.A.D. system. It must be kept in mind that for the plane-stress state considered in the numerical analysis of sheet forming processes, the porosity  $f$  must be seen as a macroscopic damage variable rather than the real fraction of void volume to matrix volume. Also it is assumed that one type of particle nucleates voids essentially at the beginning of the deformation history, giving rise to an initial porosity  $f_0$ , here taken as  $f_0=0.03$ .

The other type of particle has a distribution of nucleation strains obeying Eq.(10) with mean nucleation strain  $\epsilon_N=0.5$  and standard deviation  $S_N=0.01$  corresponding to nucleation taking place over a narrow range of strain and amplitude  $f_N=0.04$ .

For a value of the coefficient of friction  $\mu=0.12$  and a blank holder force of 70 KN, the numerical punch force curve shown on Fig.(5b) is in a very good agreement with the experimental curve displayed in Fig.(5a).

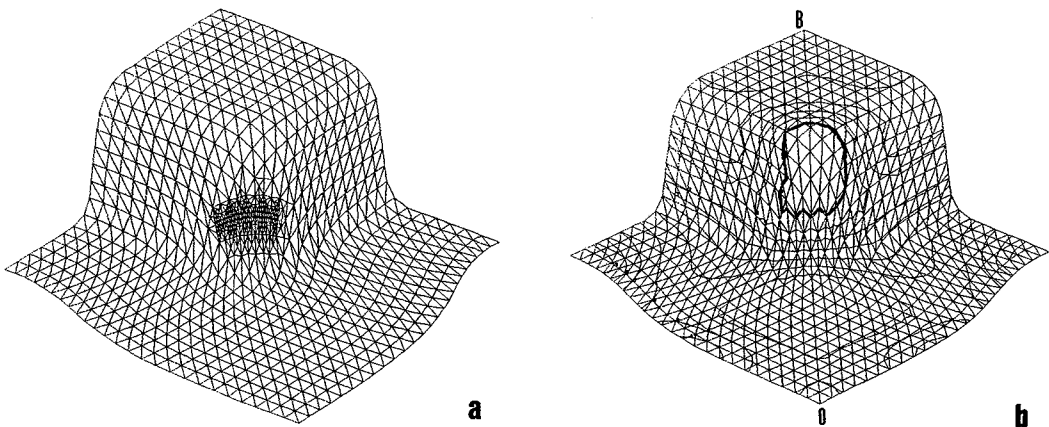


Figure 6 : (a) Adaptive mesh refinement with damage growth (b) Thickness distribution

Shown in Fig.(6a) is the adaptive mesh refinement based on the damage variable growth and localization where the maximum value  $f_{MAX}=0.0702$  coincides very well with the experimental formation of a marked thickness trough leading to fracture.

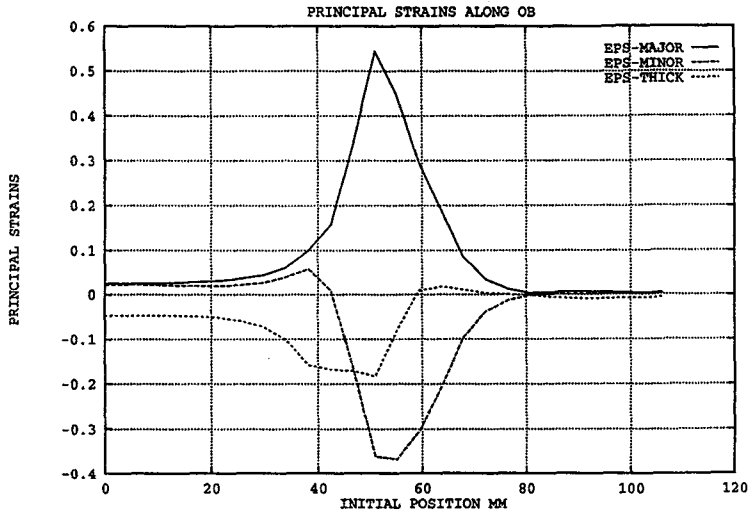


Figure 7 : Strains distribution along line OB

On the other hand, as illustrated in Fig.(6b) by the iso-values, the thickness strain distribution just before mesh refinement gives a much larger endangered area. Displayed in Fig.(7) are the principal strains distribution along line OB which may be compared to the experimental values in Fig.(4). However, we have found that the additional straining due to the coupled damage analysis is only more than 3% of major strain than that for the case without damage considered. Other numerical analyses with hemispherical punch in order to be in biaxially stretching conditions have shown the same results.

The level of the maximum damage variable depends significantly on the initial value of  $f_0$  and whether the damage variable alone may work as a localized necking criterion seems to be difficult.

We propose a numerical necking criterion based on the fact that the stress state in the neck which is localized by the damage variable is becoming triaxial. It can be shown by analyzing the triaxial stress state in the neck of a sheet undergoing plastic deformations that the stresses along the thickness direction follows the equation [14]:

$$\sigma_z = \sigma_1 [1 + \ln[1 + (a/2R)(1 - z^2/a^2)]] - \sigma_1 \quad (25)$$

where  $\sigma_1$  is the major principal stress in the neck calculated by the F.E. analysis disregarding the presence of three dimensional stress state. This stress  $\sigma_z$  varies over the thickness  $t$  of the neck, it is zero at the surface of the sheet where  $z = a = t/2$  and attains its highest value at the center of the sheet ( $z=0$ ).  $R$  is the radius of curvature of the neck in the plane containing the major principal stress. Based on experimental observations and geometrical considerations, we proposed the following simple relation for calculating the function  $a/2R$  in Eq.(25) :

$$a/2R = (t_0/l)^2 (1-t/t_0) \quad (26)$$

where  $t_0$  is the initial thickness of the sheet.  $l$  is the width of the neck in the direction of the major principal stress and  $t$  is the minimum thickness in the neck. For a precise evaluation of  $l$  and  $t$  by surface fitting, an adaptive mesh refinement in the critical area is required in the numerical analysis. Broadly speaking, the enrichment process is based on a simple side splitting operation, where-by nodes are generated in the middle of those sides that belong to elements with damage variable exceeding a given value for each remeshing procedure. Moreover, from geometrical considerations, an additional algorithm is required to ensure that nodes are connected in best possible manner.

Comparisons between numerical and experimental analysis for both deep-drawing conditions and stretching conditions have shown that typical values of the ratio  $t_0/l$  are in the range  $0.2 \leq t_0/l \leq 0.8$  and the onset of necking in the most critical area may be determined when the following stress ratio :

$$\sigma_2 \text{Max.} / \sigma_1 \geq 0.05 \quad (27)$$

and then the stress state is assumed to become triaxial in the neck. For the above square-cup deep-drawing study, a ratio  $t_0/l = 0.473$  has been found numerically for the proposed criterion. The value  $l$  may be considered a characteristic of the material dependent on the forming conditions but independent of the thickness. The following figure (8) shows the example of two deformed meshes with refinement at necking corresponding to the simulation of Marciniack's tests on a XES mild-steel sheet of thickness 0.68 mm (  $B=550.05$ ,  $c=0.9386 \text{ E-}02$ ,  $n=0.278$  and  $H=0.610$ ,  $G=0.390$ ,  $F=0.3$ ,  $N=1.4$  are the Swift's and Hill's coefficients respectively). Figure (9) displays the experimental and numerical Forming Limit Strain curves obtained where a reasonable good agreement is found.

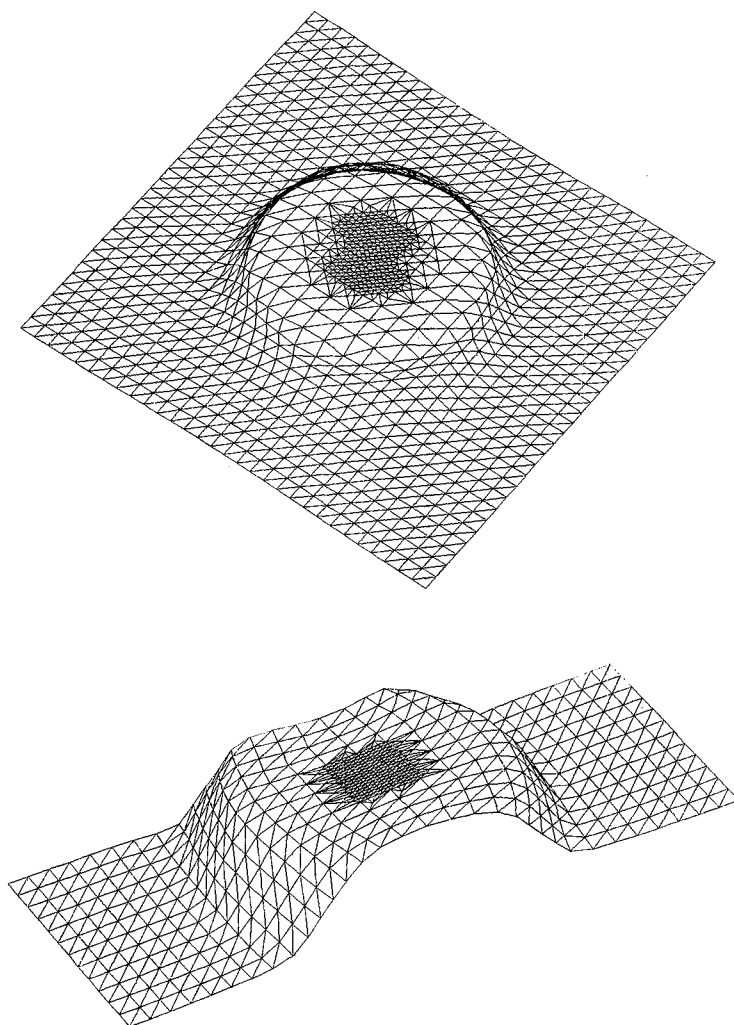


Figure (8): Deformed meshes at necking (width 150 mm and 60 mm)

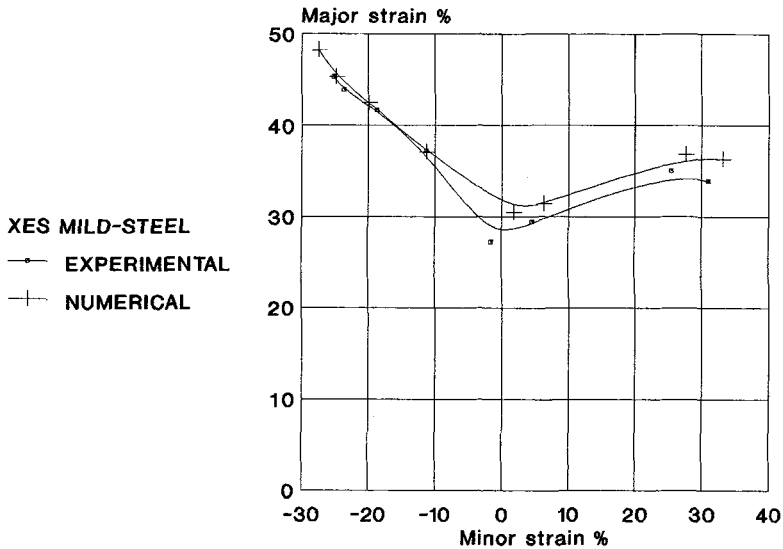


Figure (9): Forming Limit Strain Diagram

## 5. CONCLUSION

The method presented in this paper shows how the Gurson-Tvergaard's model can be extended to anisotropic sheets. The capabilities of finding localized necking by a coupled damage analysis of 3D. sheet forming processes have been demonstrated. Moreover, a necking criterion is proposed based on the fact that the stress state becomes triaxial in the neck localized by the damage variable.

## 6. REFERENCES

- [1] Brunet, M., *Materials Processing Defects*, Ed. by Ghosh, S.K. and Predeleanu, M. Elsevier Ed., (1995) 235-249
- [2] Brunet, M. Arrieux, R. and Nguyen-Nhat, T., *NUMIFORM'95*, Ed. by Shen, S.F. and Dawson, P. Balkena, A.A. ed., (1995) 669-674
- [3] Storen, S. and Rice, J.R., *J. Mech. Phys. Solids*, Vol. 123, (1975) 421-457
- [4] Yoshida, T. Katayama, T. Usuda, M., *J. of Mat. Proc. Tech.*, Vol. 50, (1995) 226-237
- [5] El-Dsoki, T. Doege, E. Groche, P., *NUMISHEET'91 VDI Bericht 894*, VDI-Verlag ed. (1991) p. 301
- [6] Doege, E. El-Dsoki, T., *J. of Mat. Proc. Tech.*, Vol. 32, N° 1-2, (1992) 127-142
- [7] Gurson, A.L., *J. Eng. Mat. Tech.* Vol. 99, (1977) 2-15
- [8] Tvergaard, V., *Int. J. Fract. Mech.* Vol. 17, (1981) 389-407
- [9] Doege, E. El-Dsoki, T. Seibert, D., *J. of Mat. Proc. Tech.*, Vol. 50, (1995) 197-206
- [10] Brunet, M. Sabourin, F., *J. of Mat. Proc. Tech.*, Vol. 50, (1995) 238-251
- [11] Aravas, N., *Int. J. Num. Meth. in Eng.* Vol. 24, (1987) 1395-1416
- [12] Sloan, S.W., *Int. J. Num. Meth. in Eng.* Vol. 24, (1987) 893-911
- [13] Chu, C.C. Needleman, A., *J. Eng. Mat. Tech.* Vol. 102, (1980) 249-256
- [14] Chaturvedi, R.C., *Materials Processing Defects*, Ed. by Ghosh, S.K. and Predeleanu, M. Elsevier Ed., (1995) 75-89